Enhancing Combustion Efficiency in Combustion Chamber: A Comparative Study of Single and Double Tangential Inlet Configurations

Wasu Suksuwan[1], Makatar Wae-hayee[1,*]

[1] Department of Mechanical Engineering, Faculty of Engineering, Prince of Songkla University, Hatyai, Songkhla, 90112, Thailand

ARTICLE INFO	ABSTRACT
	A study was conducted on a combustion chamber, with a primary focus on evaluating the influence of different air inlet configurations, specifically the single tangential inlet (ST) and double tangential inlet (DT), on combustion performance and flue gas. The feedstock was palm kernel cake, with a steady flow rate of 3 kg/hr, while the airflow is regulated to maintain an excess air ratio (EAR) of 2. The investigation encompasses temperature profiles, streamline analyses, and flue gas composition, all of which were crucial factors in assessing the combustion efficiency (C.E.) of these configurations. The results revealed distinct advantages associated with the DT configuration. It consistently demonstrated higher temperatures, symmetrical flow patterns, and improved combustion efficiency when compared to the ST setup. These findings underscore the DT configuration as a more efficient and environmentally friendly choice for combustion processes.

1. Introduction

The analysis of global primary energy consumption by fuel from 1885 to 2018 reveals intriguing trends in the energy landscape [1]. Oil has consistently dominated the energy mix as the primary fuel source, while coal, the second-largest contributor, has seen a gradual decline in usage over the years. In contrast, natural gas has ascended to become the third-largest fuel, experiencing a notable increase in demand. Hydroelectricity and nuclear energy, occupying the fourth and fifth positions, have remained relatively stable since the turn of the millennium. Notably, renewable energy, ranked sixth in 2010, has witnessed substantial growth and continues to show promising signs of expansion.

This analysis underscores the enduring dependence on fossil fuels as the primary energy source, with renewable energy emerging as a burgeoning alternative poised for further development. A key focus of this study is the potential of agricultural residues in the renewable energy sector, particularly their viability for energy conversion. In many agriculturally rich nations, agricultural residues such as rubber wood chips, coconut shell, rice husk, bagasse, and palm empty bunches [2-4] have traditionally been disposed of through burning, a practice that yields no energy benefits. Thus,

exploring methods for converting biomass into fuel presents a sustainable solution to replace fossil fuels, with biomass offering increased stability in national energy production due to its abundant and renewable nature.

The process of converting agricultural residues into usable heat energy can be categorized into three main approaches [5]: (1) Thermochemical conversion methods like pyrolysis, direct combustion, and gasification; (2) biochemical conversion processes, including fermentation and anaerobic digestion; and (3) biotechnology and nanotechnology-based processes. The choice of method depends on the desired end product, whether it be solid fuel (e.g., char, carbon), liquid fuel (e.g., biodiesel, tar, bio-oil), or gaseous fuel (e.g., biogas, synthetic gas, smoke).

Among these methods, direct combustion stands out as a straightforward and efficient means of converting agricultural waste into hot gases or steam for energy [6]. It boasts the advantage of accommodating a wide range of non-uniformly sized fuels and practical operability. However, while extensive literature [7-9] exists on various aspects of biomass combustion, there appears to be a gap in research concerning combustion of the same type of biomass in the same reactor but with different air inlet configurations.

This study seeks to address this research gap by focusing on the direct combustion of biomass within a combustion chamber employing distinct air inlet configurations, namely, the double tangential inlet (DT) and single tangential inlet (ST). The mass of biomass and velocity will be held constant as we delve into this unexplored territory to shed light on its implications for efficient biomass combustion.

2. Experimental Model

Figure 1 depicts the schematic diagram of the combustion chamber utilized in this study. The reactor has a diameter of 20 cm, standing at a total height of 150 cm. To control and measure the mass flow rate of air, a blower is employed, accelerating the air as it traverses the orifice flow meter. The blower's rotational speed is regulated using an inverter to ensure precise control.

A notable feature of this setup is the implementation of double air inlet pipes, a configuration carefully designed based on previous research [10]. These pipes are characterized by an inner diameter of 46.8 mm and are strategically connected tangentially to the bottom of the reactor. This design promotes a swirling flow pattern within the reactor, which has significant implications for the combustion process.

Within the reactor, there is a mechanism for controlling both the air inlet and the feeding of fuel. These controls are adjusted in accordance with the excess air ratio, a critical factor influencing the composition of the flue gas. The composition gas then ascends to the top of the reactor and proceeds through a two-stage cyclone system.

The first cyclone serves the purpose of separating gas from larger dust particles, ensuring that the gas leaving the system is free from such contaminants. The second cyclone further refines this process, filtering out smaller dust particles before allowing the cleaned gas to be released into the environment. Any dust and fine particles collected in each cyclone are safely deposited into an ash storage box for disposal. This meticulous setup ensures efficient combustion and minimizes environmental emissions during the process.
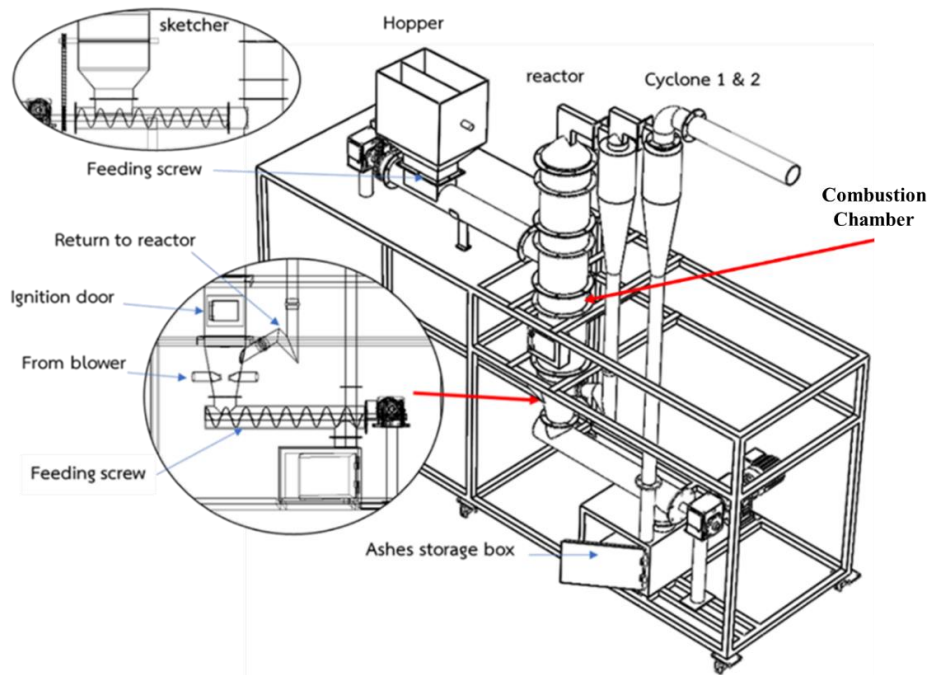
Fig. 1. Schematic diagram of combustion chamber

In this study, the primary feedstock utilized is palm kernel cake, sourced from the palm oil milling operations of our research team. The feedstock is carefully prepared, with its size reduced to less than 10 mm, providing an optimal size for the gasification process. The feeding process commences with a consistent flow rate of 3 kg/hr, facilitated by a screw conveyor, ensuring a steady supply of feedstock to the reactor. Simultaneously, the flow rate of air is regulated to maintain an excess air ratio (EAR) = 2. The calculation for excess air ratio [11] is determined using the following equation:

$$\text{Excess Air ratio (EAR)} = \frac{\text{Actual air supply}}{\text{Air demand at stoichiometric condition}} \tag{1}$$

To monitor the combustion process accurately, Type-S and Type-K thermocouples were strategically positioned along the central height of the combustion chamber. Figure 1 illustrates the six specific locations within the combustion chamber where temperature measurements were taken. Among these positions, two Type-S thermocouples were installed within the burning zone of the chamber, chosen due to their exposure to high temperatures.

Additionally, four Type-K thermocouples were strategically placed at different heights within the upper section of the combustion chamber. This comprehensive placement of thermocouples enabled the precise measurement of temperature variations at various points within the chamber.

To minimize heat loss and maintain optimal combustion conditions, the combustion chamber was effectively insulated using high-temperature insulation material, specifically KAOWOOL ASK-7912-H 8P Blanket, rated for temperatures up to 1,400°C.

Throughout the combustion process, temperature readings at the six specified positions within the combustion chamber were recorded at one-minute intervals using a datalogger. Furthermore, to ensure the quality of the flue gas, the gas was subjected to a cleaning process involving a water scrubber [12,13]. To evaluate the combustion quality of the flue gas, the concentration of carbon dioxide (CO_2), oxygen (O_2), and carbon monoxide (CO) in the flue gas was meticulously measured using a gas analyser. This parameter serves as a crucial indicator of the combustion efficiency.

3. Numerical Simulation Model

3.1 Computational Model and Boundary Conditions

In order to replicate the experimental setup of the circulating fluidized bed gasifier, a 3-D numerical model was meticulously designed using the commercial CFD software, ANSYS (Fluent). This numerical model closely mimicked the physical reactor used in the experiments, maintaining the same dimensions. The specifics of the boundary conditions employed in this numerical model are concisely summarized in Figure 2 and Table 1. Boundary conditions were applied at four distinct boundaries within the model. Notably, the air inlet was positioned in a tangential manner, integrated into the divergent section of the reactor. This connection point was situated at a height of 15 cm from the bottom of the reactor. The fuel inlet was situated at the bottom of the reactor, and the air outlet was located at the reactor's top. The reactor's surface was defined as a solid wall.

Table 1
The details of boundary conditions

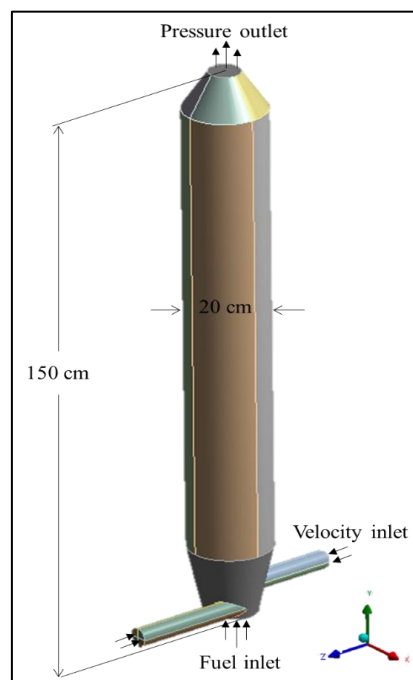| Boundary condition	Define
Air inlet	Velocity inlet
Air outlet	Pressure outlet
Fuel inlet	Fuel inlet
Surfaces of reactor	Wall

Fig. 2. Computational model and boundary conditions

3.2 Grid Generation and Grid Dependency

Figure 3 illustrates the numerical model of the swirling fluidized bed, primarily structured as a rectangular grid. The grid generation was meticulously tailored for various regions within the model. Here is a breakdown of the grid design strategy: Conical region (bottom of reactor), a finer grid was specifically generated for the conical region at the bottom of the reactor. This decision was driven by the considerably higher velocities observed in this part. Middle of reactor, in the central section of

the reactor, the grid was intentionally designed to be coarser compared to other areas. This choice aligns with the specific characteristics of this region and also takes computational efficiency into account, and top and bottom of reactor: finer grid resolution was applied to both the top and bottom regions of the reactor compared to the middle section. This finer grid resolution is crucial for capturing the intricate details and phenomena occurring at these critical locations.

Drawing from findings in a prior study [14,15] we systematically varied the number of generated grid elements within the range of 0.10 to 3.54 million elements. This exploration aimed to assess grid dependency and its impact on numerical solution accuracy. The outcomes of these investigations led us to option for 1.71 million grid elements in the previous study. This selection struck an optimal balance between achieving highly accurate results while managing computational costs effectively.
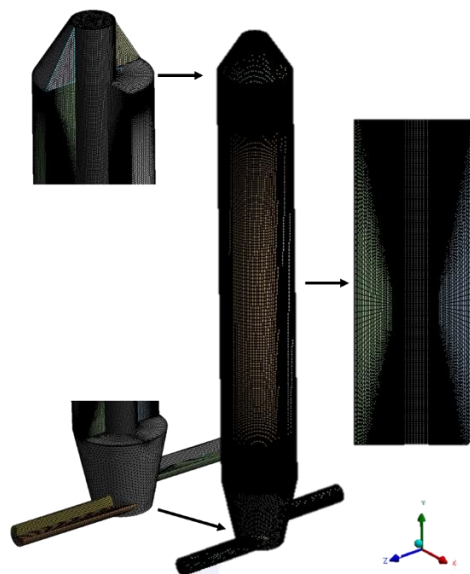

Fig. 3. Generated rectangular grid for the numerical model

3.3 Calculation Method and Algorithm

The computations in this study involved the solution of the Reynolds-averaged continuity and Navier-Stokes equations, all while adhering to specific boundary conditions. This turbulence model has been widely adopted for numerous numerical simulations of internal flow, demonstrating its proficiency in predicting internal flow solutions with a reasonable computational cost [16,17].

In the context of radiation modelling, the Discrete Ordinate (DO) model was employed for this work. Additionally, a species transport model was utilized, with proximate and ultimate analyses of palm kernel cake as defined in this model. The numerical scheme employed in this study involves the SIMPLE (Semi-Implicit Method for Pressure-Linked Equations) algorithm. This algorithm is coupled with an upwind scheme, and it's worth noting that two distinct upwind schemes were utilized. The first-order upwind scheme was applied to turbulent kinetic energy, turbulent dissipation rate, and discrete ordinates. On the other hand, the second-order upwind scheme was utilized for variables such as pressure, momentum, volume, and energy.

To ensure the convergence of the iterative solution, it was deemed successful when the residuals of all the variables reached values below a specified threshold. In this study, the specified threshold for all residuals was set at 1×10^{-4}. This stringent criterion helps ensure the accuracy and reliability of the computed results [18,19].

4. Results and Discussion

4.1 Temperature Profiles of Experiment Test and Numerical Studies

In Figure 4, both the temperature profile from experimental tests and the temperature contour from numerical simulations are presented. This analysis focused on investigating the effects of different air configurations, specifically the double tangential inlet (DT) and single tangential inlet (ST), while maintaining a constant EAR = 2 and a fixed mass flow rate of 3 kg/h.

The temperature profiles depicted in Figure 4(a) clearly indicate that the temperature profiles associated with the double tangential inlet (DT) configuration were notably higher compared to those of the single tangential inlet (ST) configuration. Notably, at a position corresponding to H = 0.25 m, the maximum temperature along the reactor was observed for both air configurations. This specific point marks the combustion zone, where the highest temperatures are attained. Moving upwards in the reactor, the temperature profiles gradually decreased until reaching H = 1.05 m. At H = 1.35 m, a slight increase in temperature was observed. This temperature rise is attributed to the top of the reactor, which takes on a conical shape and is directly connected to the cyclone section of the system. This unique configuration has a distinct impact on temperature distribution within the reactor.

In Figure 4(b), which presents the temperature contour from numerical simulations, it's evident that the temperature contour associated with the double tangential inlet (DT) configuration exhibited higher temperatures compared to the single tangential inlet (ST) configuration. This observation aligns with the findings from the experimental studies.

Specifically, in the case of the ST configuration, the temperature contour indicates that the highest temperature region is situated at the bottom of the reactor. However, it's noteworthy that this highest-temperature zone appears relatively small in size.

Conversely, when examining the temperature contour of the DT configuration, a different pattern emerges. Here, the combustion zone is notably visible at the side of the chamber. As the chamber height increases, this combustion zone gradually combines and canters within the chamber.

This contrasting temperature distribution between the ST and DT configurations highlights the distinct combustion dynamics and temperature profiles associated with these two air inlet configurations.
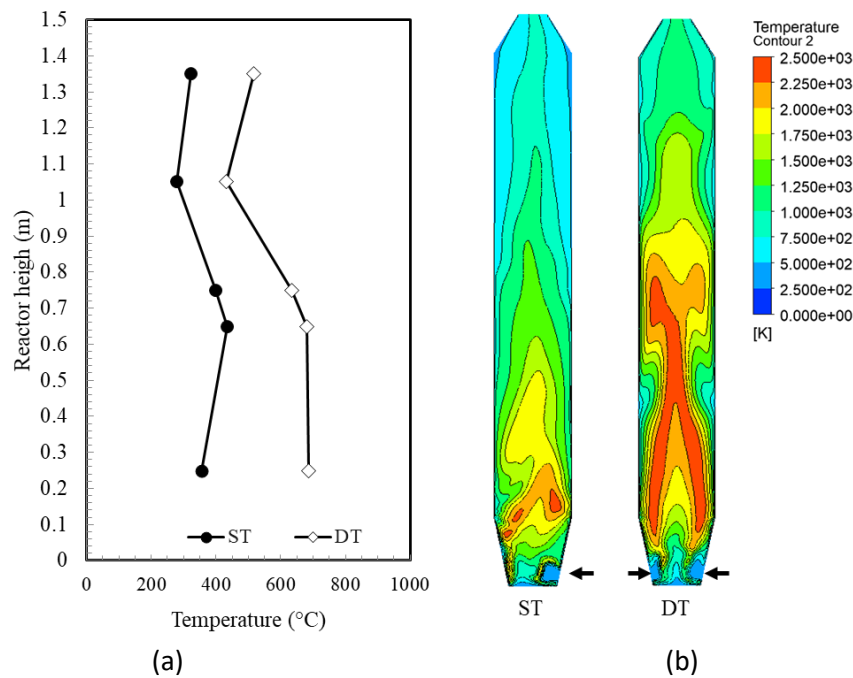
Fig. 4. Temperature profiles of experiment test and temperature contour of numerical studies: (a) Temperature profiles; (b) Contour of temperature

Figure 5 presents the streamline visualization of the combustion chamber, derived from the results of numerical simulations. These visualizations offer valuable insights into the flow patterns within the chamber for different air inlet configurations.

In the case of the single tangential inlet (ST) configuration, the streamline visualization reveals high-velocity flow concentrated on one side at the bottom of the chamber. This concentrated flow is a consequence of having a single air inlet. As the chamber height increases, the streamlines exhibit a turbulent flow pattern, signifying the dynamic behaviour of the combustion process in this configuration.

Conversely, for the double tangential inlet (DT) configuration, the streamline visualization demonstrates a symmetrical flow pattern on both sides of the chamber. This symmetry is a result of the double air inlets, which work to evenly disperse the flow around the chamber. This balanced flow distribution is a critical factor contributing to the creation of a wider combustion zone.

The distinct flow characteristics between the ST and DT configurations emphasize how the choice of air inlet configuration significantly influences the flow dynamics within the combustion chamber. In the case of the DT configuration, the symmetrical flow pattern plays a pivotal role in achieving a broader and more evenly distributed combustion zone.
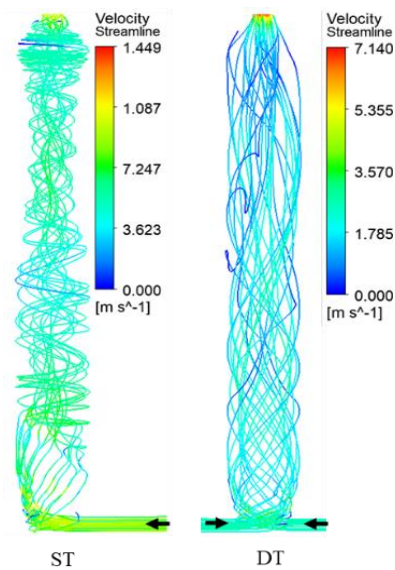
Fig. 5. Velocity streamlines of numerical studies

4.2 Flue Gas

Figure 6 provides an insightful depiction of the flue gas rate concentration for both the single tangential inlet (ST) case, illustrated in Figure 6(a), and the double tangential inlet (DT) case, as shown in Figure 6(b).

In the case of DT, it's evident from the results that the flue gas rate exhibits a steadier behaviour compared to the ST configuration. This observed stability is closely tied to the flow pattern within the chamber, as previously discussed in the streamline results.

For the ST configuration, the results indicate a less steady composition of flue gas over time. Initially, the O_2 concentration is higher, followed by a decrease in O_2 levels while CO and CO_2 concentrations increase. This fluctuation reflects the dynamic nature of the combustion process in the ST configuration.

Conversely, in the DT case, the flue gas rate curve appears smoother, suggesting a more stable combustion process. Interestingly, the relationship between O_2, CO, and CO_2 concentrations in the DT case mirrors that of the ST case.

These observations underscore the significant impact of the chosen air inlet configuration on the stability and characteristics of the flue gas composition during the gasification process. The DT configuration appears to offer more consistent and predictable results compared to the ST configuration, which exhibits more fluctuations in gas composition over time.
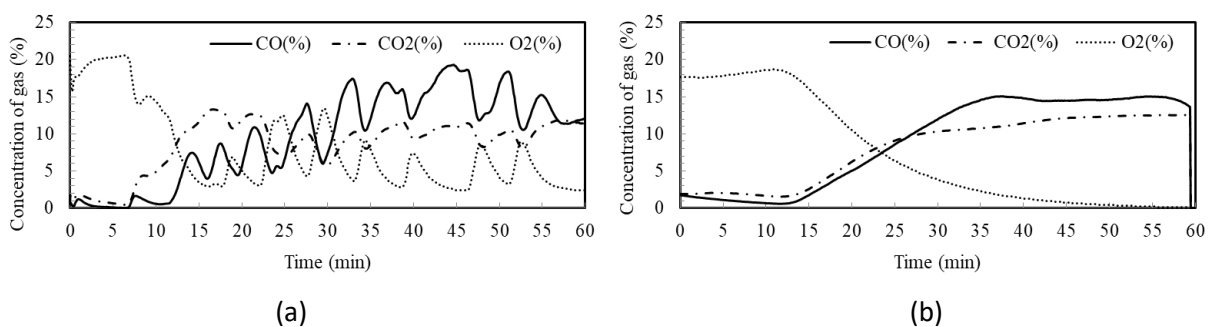

(a)   (b)

Fig. 6. Concentration of flue gas rate: (a) ST; (b) DT

To facilitate a more meaningful comparison between the compositions of flue gas from the single tangential inlet (ST) and double tangential inlet (DT) configurations, an analysis was conducted to determine the average concentrations of flue gas within the time range of 30 minutes to 60 minutes, as demonstrated in Figure 7.
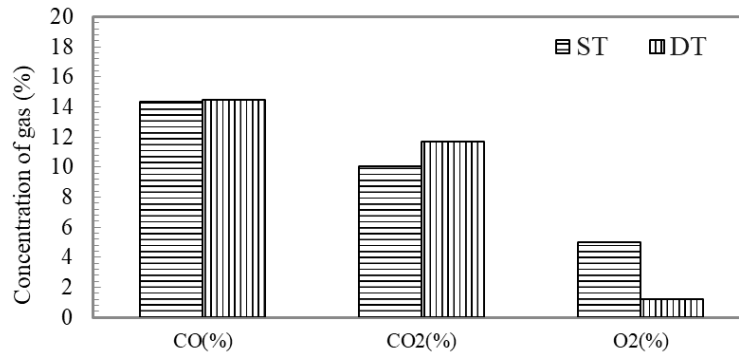

Fig. 7. Concentration of flue gas

The analysis reveals that the carbon monoxide (CO) concentration in both ST and DT configurations was quite similar, with both hovering around 14%. However, it's worth noting that this slight difference may not be substantial.

In contrast, the carbon dioxide (CO_2) concentration was notably higher in the DT configuration, at approximately 12%, compared to the ST configuration, which recorded around 10%. This discrepancy suggests that the DT configuration achieved a closer-to-complete combustion compared to the ST configuration. Higher CO_2 levels are indicative of more efficient combustion.

Furthermore, the oxygen (O_2) concentration in the DT configuration was lower, indicating that a significant portion of oxygen was consumed in the combustion process. This consumption of oxygen is consistent with more effective combustion.

In summary, the analysis of the average concentrations of flue gas provides a clearer picture. It indicates that the DT configuration tends to achieve more efficient and complete combustion compared to the ST configuration, with higher CO_2 levels and lower O_2 levels reflecting this difference in combustion performance.

4.3 Combustion Efficiency (C.E)

Regarding emissions, the concentrations of carbon monoxide (CO) and carbon dioxide (CO_2) in the flue gas are depicted in Figure 7. These parameters are vital in assessing the combustion efficiency (C.E.) [20].

$$C.E. = \frac{[CO_2]}{[CO_2] + [CO]} \; x \; 100\% \tag{2}$$

Certainly, based on Eq. (2) where CO_2 is volume concentration of CO_2, CO represents the volume concentration of carbon monoxide (CO), the combustion efficiency (C.E.) can be calculated. The results are presented in Figure 8.

The analysis reveals that for the single tangential inlet (ST) configuration, the combustion efficiency (C.E.) was approximately 41%. In contrast, for the double tangential inlet (DT) configuration, the combustion efficiency (C.E.) was around 45%. These results clearly indicate that the DT configuration achieved a higher combustion efficiency compared to the ST configuration.

This difference in combustion efficiency suggests that the DT configuration is more effective in converting fuel into carbon dioxide (CO2) and reducing carbon monoxide (CO) emissions, making it a preferable choice for achieving better combustion performance.
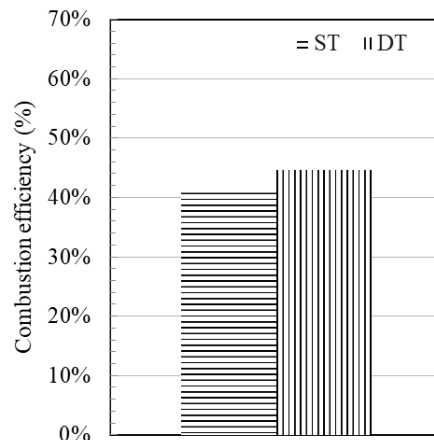

Fig. 8. Combustion efficiency of flue gas

4. Conclusions

In conclusion, this study has delved into the performance of a combustion chamber, particularly focusing on the impact of different air inlet configurations, namely the single tangential inlet (ST) and double tangential inlet (DT), on the combustion process and flue gas. The key findings and conclusions of this research can be summarized as follows:

- Temperature profiles: the temperature profiles in the combustion chamber revealed that the DT configuration consistently exhibited higher temperatures compared to the ST configuration. This temperature distribution is essential for achieving efficient combustion.
- Streamline analysis: streamline visualizations demonstrated that the DT configuration produced a more symmetrical and evenly distributed flow within the chamber. This balanced flow pattern contributed to a wider and more stable combustion zone.
- Flue gas composition: the flue gas composition analysis indicated that the DT configuration resulted in a more steady and closely complete combustion process. Specifically, it showed higher carbon dioxide (CO_2) levels and lower oxygen (O_2) concentrations, reflecting better combustion efficiency.
- Combustion efficiency: calculations of combustion efficiency (C.E.) further confirmed that the DT configuration outperformed the ST configuration. The DT setup achieved a higher C.E., signifying superior combustion performance.

In summary, the double tangential inlet (DT) configuration consistently demonstrated superior performance in terms of temperature distribution, flow patterns, flue gas composition, and combustion efficiency. This configuration is recommended for achieving efficient and combustion processes.

Acknowledgement

References

[1] Petroleum, British. "Statistical Review of World Energy 2019 (68)." (2019).
[2] Kaewluan, Sommas, and Suneerat Pipatmanomai. "Preliminary study of rubber wood chips gasification in a bubbling fluidised-bed reactor: Effect of air to fuel ratio." In *Proceedings of the PSU-UNS International Conference on Engineering and Environment, Phuket, Thailand*, pp. 10-11. 2007. https://doi.org/10.1007/978-3-540-76694-0_236
[3] Promdee, Kittiphop, Jirawat Chanvidhwatanakit, Somruedee Satitkune, Chakkrich Boonmee, Thitipong Kawichai, Sittipong Jarernprasert, and Tharapong Vitidsant. "Characterization of carbon materials and differences from activated carbon particle (ACP) and coal briquettes product (CBP) derived from coconut shell via rotary kiln." *Renewable and Sustainable Energy Reviews* 75 (2017): 1175-1186. https://doi.org/10.1016/j.rser.2016.11.099
[4] Konsomboon, Supatchaya, Suneerat Pipatmanomai, Thanid Madhiyanon, and Suvit Tia. "Effect of kaolin addition on ash characteristics of palm empty fruit bunch (EFB) upon combustion." *Applied Energy* 88, no. 1 (2011): 298-305. https://doi.org/10.1016/j.apenergy.2010.07.008
[5] Basu, Prabir. *Biomass gasification and pyrolysis: practical design and theory*. Academic press, 2010.
[6] Wilk, Veronika, Hannes Kitzler, Stefan Koppatz, Christoph Pfeifer, and Hermann Hofbauer. "Gasification of waste wood and bark in a dual fluidized bed steam gasifier." *Biomass conversion and biorefinery* 1 (2011): 91-97. https://doi.org/10.1007/s13399-011-0009-z
[7] Elmay, Yassine, Mejdi Jeguirim, Sophie Dorge, Gwenaëlle Trouvé, and Rachid Said. "Evaluation of date palm residues combustion in fixed bed laboratory reactor: A comparison with sawdust behaviour." *Renewable energy* 62 (2014): 209-215. https://doi.org/10.1016/j.renene.2013.07.007
[8] Qian, F. P., Chien-Song Chyang, K. S. Huang, and Jim Tso. "Combustion and NO emission of high nitrogen content biomass in a pilot-scale vortexing fluidized bed combustor." *Bioresource Technology* 102, no. 2 (2011): 1892-1898. https://doi.org/10.1016/j.biortech.2010.08.008
[9] Kluska, Jacek, Tomasz Turzyński, Mateusz Ochnio, and Dariusz Kardaś. "Characteristics of ash formation in the process of combustion of pelletised leather tannery waste and hardwood pellets." *Renewable energy* 149 (2020): 1246-1253. https://doi.org/10.1016/j.renene.2019.10.122
[10] Suksuwan, Wasu, Mohd Faizal Mohideen Batcha, Arkom Palamanit, and Makatar Wae-hayee. "The Effect of Biomass Shapes on Combustion Characteristic in Updraft Chamber." *International Journal of Integrated Engineering* 13, no. 4 (2021): 163-171.
[11] Wang, Yu, Yixin Shao, Miodrag Darko Matovic, and Joann K. Whalen. "Exploring switchgrass and hardwood combustion on excess air and ash fouling/slagging potential: Laboratory combustion test and thermogravimetric kinetic analysis." *Energy Conversion and Management* 97 (2015): 409-419. https://doi.org/10.1016/j.enconman.2015.03.070
[12] Dufour, Anthony, P. Girods, E. Masson, Y. Rogaume, and A. Zoulalian. "Synthesis gas production by biomass pyrolysis: effect of reactor temperature on product distribution." *international journal of hydrogen energy* 34, no. 4 (2009): 1726-1734. https://doi.org/10.1016/j.ijhydene.2008.11.075
[13] Woolcock, Patrick J., and Robert C. Brown. "A review of cleaning technologies for biomass-derived syngas." *Biomass and bioenergy* 52 (2013): 54-84. https://doi.org/10.1016/j.biombioe.2013.02.036
[14] Suksuwan, Wasu, Mohd Faizal Mohideen Batcha, Arkom Palamanit, and Makatar Wae-hayee. "Experimental and Numerical Studies of Combustion Characteristics in Swirling Fluidized Bed Gasifier Using Palm Cake as Feedstock." In *IOP Conference Series: Earth and Environmental Science*, vol. 765, no. 1, p. 012069. IOP Publishing, 2021. https://doi.org/10.1088/1755-1315/765/1/012069
[15] Suksuwan, Wasu, Makatar Wae-hayee, and Maizirwan Mel. "The Effect of Single and Double Air Inlets on Swirling Flow in a Reactor of a Fluidized Bed Gasifier." *Journal of Advanced Research in Fluid Mechanics and Thermal Sciences* 44, no. 1 (2018): 157-166.
[16] Singh, Ravi Inder, Anders Brink, and Mikko Hupa. "CFD modeling to study fluidized bed combustion and gasification." *Applied thermal engineering* 52, no. 2 (2013): 585-614. https://doi.org/10.1016/j.applthermaleng.2012.12.017

[17] Adamczyk, Wojciech P., Paweł Kozołub, Adam Klimanek, Ryszard A. Białecki, Marek Andrzejczyk, and Marcin Klajny. "Numerical simulations of the industrial circulating fluidized bed boiler under air-and oxy-fuel combustion." *Applied Thermal Engineering* 87 (2015): 127-136. https://doi.org/10.1016/j.applthermaleng.2015.04.056

[18] Chen, Juhui, Weijie Yin, Shuai Wang, Cheng Meng, Guangbin Yu, Ting Hu, and Feng Lin. "Analysis of biomass gasification in bubbling fluidized bed with two-fluid model." *Journal of Renewable and Sustainable Energy* 8, no. 6 (2016). https://doi.org/10.1063/1.4967717

[19] Raza, Naveed, Muhammad Ahsan, Muhammad Taqi Mehran, Salman Raza Naqvi, and Iftikhar Ahmad. "Computational analysis of the hydrodynamic behavior for different air distributor designs of fluidized bed gasifier." *Frontiers in Energy Research* 9 (2021): 692066. https://doi.org/10.3389/fenrg.2021.692066

[20] Wu, Kuo-Kuang, Yu-Cheng Chang, Chiun-Hsun Chen, and Young-Da Chen. "High-efficiency combustion of natural gas with 21–30% oxygen-enriched air." *Fuel* 89, no. 9 (2010): 2455-2462. https://doi.org/10.1016/j.fuel.2010.02.002